Temperature dependence of the nuclear quadrupole interaction at Zr-Ti sites in $PbZr_xTi_{(1-x)}O_3$ in the Zr-rich rhombohedral and cubic phases

1998 J. Phys.: Condens. Matter 10 2139

(http://iopscience.iop.org/0953-8984/10/9/017)

J. Phys.: Condens. Matter **10** (1998) 2139–2153. Printed in the UK PII: S0953-8984(98)86460-6

Temperature dependence of the nuclear quadrupole interaction at Zr–Ti sites in $PbZr_xTi_{(1-x)}O_3$ in the Zr-rich rhombohedral and cubic phases

R E Alonso, A López García, A Ayala and P de la Presa

Programa TENAES, Departamento de Física, Facultad de Ciencias Exactas, Universidad Nacional de La Plata CC-67, 1900 La Plata, Argentina

Received 28 July 1997, in final form 17 October 1997

Abstract. In this paper, the hyperfine quadrupole interaction at the Zr–Ti site of $PbZr_xTi_{(1-x)}O_3$ (PZT) polycrystalline samples is studied for the first time. Powders for $x = 0$, 0.1, 0.2, 0.4, 0.6, 0.8, 0.9 and 1 were prepared and characterized by XRD. The lattice constants and space groups were obtained as functions of Ti concentration. PAC analyses were done for ferroelectric PZT for $x = 0.9$ and 0.8 as a function of temperature, and for $x = 0.6$ at RT. Also antiferroelectric $PbZrO_3$ was analysed. Low-concentration ^{181}Ta nuclei were used as probes. In the ferroelectric and paraelectric phases of PZT compounds two sites were occupied by probes. For each site the quadrupole frequency, asymmetry and relative distribution width parameters were obtained as functions of temperature above and below the Curie temperature. For $PbZrO_3$ only one site was detected with a static quadrupole interaction below T_c and a nuclear spin-relaxation process above it. Furthermore, the temperature dependence of the hyperfine parameters, the possible origin of both quadrupole interactions in PZT and the perturbation that characterizes the cubic phases of ABO_3 and $ABB'O_3$ compounds are discussed.

1. Introduction

Due to their ferroelectric and piezoelectric properties, solid solutions of $Pb(Ti, Zr)O_3$ have been used in many applications in microelectronics. It was in the 1950s that the ferroelectric characteristic of PZT was first observed in Japan. Many studies using different techniques have established the macroscopic properties of powder samples as well as of thin-film specimens. Solid solutions of $PbZr_xTi_{(1-x)}O_3$ crystallize in the perovskite structure. In figure 1 we can see the phase diagram as a function of Ti concentration. Part of this diagram was originally proposed by Shirane *et al* [1, 2], and Sawaguchi *et al* [3]. Later, electrical measurements reported by Barnett [4] indicated that the ferroelectric rhombohedral (FR) region of the solid solution probably consisted of two different phases. In 1969 Michael *et al* [5], using neutron diffraction patterns, found different structures that were called FR(LT) and FR(HT), respectively. These authors observed in a 10% Ti concentration FR(LT) sample the presence of a superstructure at RT and proposed a model, in which the primitive unit cell contains two formula units with alternating clockwise and anticlockwise tilts of the oxygen octahedra. This makes the size of the unit cell double that of the prototype perovskite cell along [111]. It was established that the FR(LT) structure has the space group $R3c$ and that the FR(HT) structure has the space group $R3m$. In 1977 Glazer *et al* [6] made neutron scattering analysis of the property changes as functions of the temperature for $PbZr_{0.9}Ti_{0.1}O_3$ and showed that the oxygen tilts disappear in the transition from the FR(LT) structure to

0953-8984/98/092139+15$19.50

the FR(HT) structure. In the work of Ito *et al* [7] and Glazer *et al* [6] it is shown that the combination of neutron diffraction and profile analysis with x-ray diffraction can deal with the very tiny distortions of the ideal perovskite structure (i.e. ion position displacements and oxygen octahedron tilts) that make these materials ferroelectric. With the knowledge of atomic positions and phase characterizations, many models have been applied to these and other perovskite-type compounds, in efforts to understand the origin of the ferroelectricity and the nature of the phase transitions. Although the perovskite-type compounds are simple in their atomic structure, it is still not clear whether the phase transitions have displacive or dynamic character [8, 9].

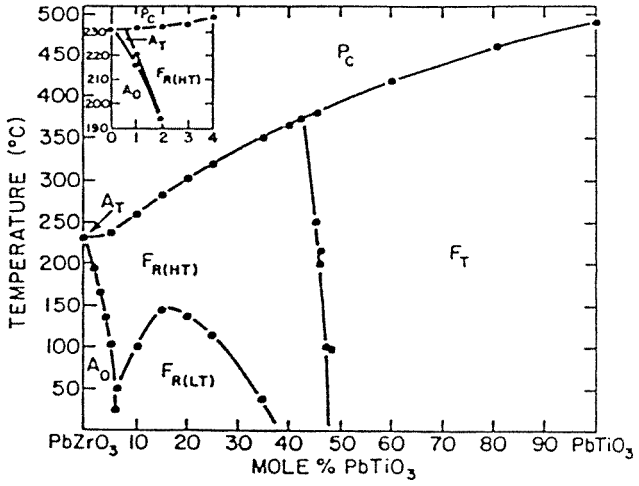

Figure 1. The phase diagram of PZT as a function of Ti concentration. From references [1–3].

In this work we present for the first time a hyperfine analysis of PZT using perturbed angular correlation (PAC) spectroscopy. This technique allows a microscopic study to be made of the charge distributions surrounding probes that are incorporated into the sample at a very low concentration. As a result we can deduce the electric field gradient (EFG) tensor at the sites occupied by the probes, which gives information about the electric charge distribution in their vicinity. The aim of this work is to study the evolution of the EFG as a function of temperature and to achieve an understanding of the microscopic properties of these materials.

2. Experimental procedure

2.1. Sample preparation

For the XRD and PAC analyses, samples of $PbZr_xTi_{(1-x)}O_3$ for $x = 0$, 0.1, 0.2, 0.4, 0.6, 0.8, 0.9 and 1 were prepared by the solid-state reaction technique. Powder samples were obtained by mixing stoichiometric quantities of PbO (Johnson–Matthey Chemicals Grade I, 99.99% purity), ZrO_2 (Fluka Chemie AG, 99% purity with ∼3% of HfO_2) and TiO_2 (Riedel–de Haen, 99.5% purity) in a PbO atmosphere to form the desired $PbZr_xTi_{(1-x)}O_3$ solutions.

The 'as-prepared' mixtures were sequentially ground and calcined at temperatures of 773, 1073 and 1273 K. The calcination time at each temperature was 6 h. Care was taken to avoid higher temperatures because it was observed that these compounds dissociated at

about 1373 K. The thermal evolution of each material was controlled by XRD analysis. The diffraction pattern showed that the different PZT samples were almost completely formed after the calcination at 1073 K. For the PAC study we used ^{181}Ta as the probe. It was produced by thermal neutron irradiation of ^{180}Hf contained in the samples as an impurity in naturally abundant zirconium. The samples were irradiated with a flux of 2×10^{13} neutrons cm^{-2} s^{-1} for 7 h at approximately 60 °C. The ^{181}Ta concentration was less than ppm.

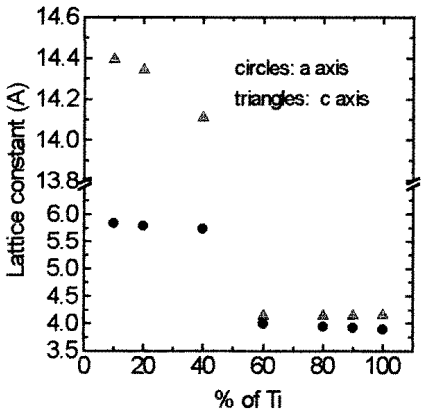

Figure 2. The lattice constants at RT as functions of Ti concentration. For PZT 6040 the *c*-axis lattice parameter is doubled.

2.2. XRD characterization

The 'as-prepared' powder samples were characterized at RT by x-ray diffraction analysis. Refinement was carried out with the Rietveld program AT RSS-92. The variables were: an overall scale factor, three half-width parameters defining the Gaussian line shapes, isotropic temperature factors, the atomic position parameters, the unit-cell parameters, the coefficients of a third-order background polynomial and the offset of the 2θ zero point. No effect was observed upon freeing the preferred orientation, asymmetry and texture parameters. With this procedure, we obtained the unit-cell parameters and established the correct space group. Moreover, the analysis of the spectra enables us to discard the possibility of the presence of other compounds. In figure 2 we show the variations of the lattice parameters as functions of titanium concentration. We determined that the compounds with $x = 0.9$ and 0.8 had the space groups $R3c$, that with $x = 0.6$ had the space group $R3m$ and those with $x = 0.4$, 0.2, 0.1 and 0 had the space group $P4mm$, in good agreement with previous reports [4–6, 9]. For the rhombohedral phase, the value of the *c*-axis lattice parameter is referred to as the hexagonal double-unit-cell parameter [7]. Although the *c*-axis lattice parameter for $PbZr_{0.6}Ti_{0.4}O_3$ is not doubled because the superstructure presumably exists below RT, the *c*-axis lattice parameter for this concentration has been multiplied by 2 to allow direct comparison of its FR(HT) value at RT with those corresponding to the other concentrations, also at RT. In this figure it can also be seen that the cell parameters decrease while titanium substitution increases, due to the smaller ionic radius of titanium compared to that of zirconium.

2.3. PAC spectroscopy

The angular correlation function of a gamma–gamma cascade, $W(\vartheta, t)$, whose intermediate nuclear state has a quadrupole moment Q that interacts with a local electric field gradient tensor (EFG) and therefore is modulated by means of the perturbation factors $G_{kk}(t)$, is given [10] by

$$W(\vartheta, t) = 1 + A_{22}G_{22}(t)P_2(\cos\vartheta) + A_{44}G_{44}(t)P_4(\cos\vartheta) + \cdots \tag{1}$$

where

$$G_{kk}(t) = \sum f_s G^s_{kk}(t). \tag{2}$$

In the last expression f_s is the fraction of perturbed nuclei at site s and G^s_{kk} is the perturbation factor corresponding to those nuclei at this site. The sum is over the number of available sites s.

For static quadrupole interactions and nuclei with spin $I = 5/2$, these factors have the form

$$G_{kk}(t) = \sigma_{k0} + \sum \sigma_{kn}\cos(\omega_n t)\exp(-\omega_n \delta t) \tag{3}$$

where the sum runs from $n = 1$ to $n = 3$ and the frequencies ω_n are related to the energy splitting that arises when the nuclear quadrupole moment interacts with an electric field gradient tensor. These frequencies are functions of the quadrupole frequency $\omega_q = e^2V_{zz}Q/4I(2I-1)\hbar$ and the asymmetry parameter $\eta = (V_{yy} - V_{xx})/V_{zz}$. In the last two expressions, V_{zz} is the major principal-axis component of the EFG tensor, which obeys the Laplace equation together with the other diagonal components: $V_{xx} + V_{yy} + V_{zz} = 0$. The coefficients σ_{kn} are known functions of η. For ^{181}Ta, $Q = 2.53 \times 10^{-24}$ cm^2 is the quadrupole moment of the intermediate nuclear state of the 133–482 keV gamma–gamma cascade [11]. The attenuation in the oscillation amplitude introduced in the right-hand side of equation (2) through the relative width parameter δ takes into account the frequency distribution with Lorentzian shape around the central value ω_q. These distributions are included to describe lattice imperfections.

For a time-dependent hyperfine electric quadrupole interaction, the Abragam and Pound relaxation model valid for a fast relaxation process is used [12]:

$$G_{22}(t) = \mathrm{e}^{-\lambda t} \tag{4}$$

where the relaxation parameter λ is proportional to the mean squared value of the EFG and the correlation time.

2.4. The experimental set-up and data fit

The time spectra were measured with a two-CsF-detector set-up, storing coincidence data at 90°, 180° and 270°. The spectrometer has a time resolution of 0.7 ns for the 133–482 keV gamma–gamma cascade of ^{181}Ta. The coincidence spectra at every temperature were obtained after an accumulation time of one day or more. For the measurement of the angular correlation spectra as functions of temperature the samples were heated *in situ* in a furnace with a thermal stability better than 1 K. The anisotropy versus time or spin-precession curve is obtained from the expression

$$A_{22}G_{22}(t) = 2[C(180, t) - C(90, t)]/[C(180, t) + 2C(90, t)] \tag{5}$$

where $C(90, t)$ and $C(180, t)$ are the coincidence counts measured at time t with angles between the detectors of 90° and 180°, respectively. For the determination of the hyperfine parameters ω_q, η and δ or λ, least-squares fits with the appropriate functions (equations (2), (3) or (4)) to the experimental results (equation (5)) were performed.

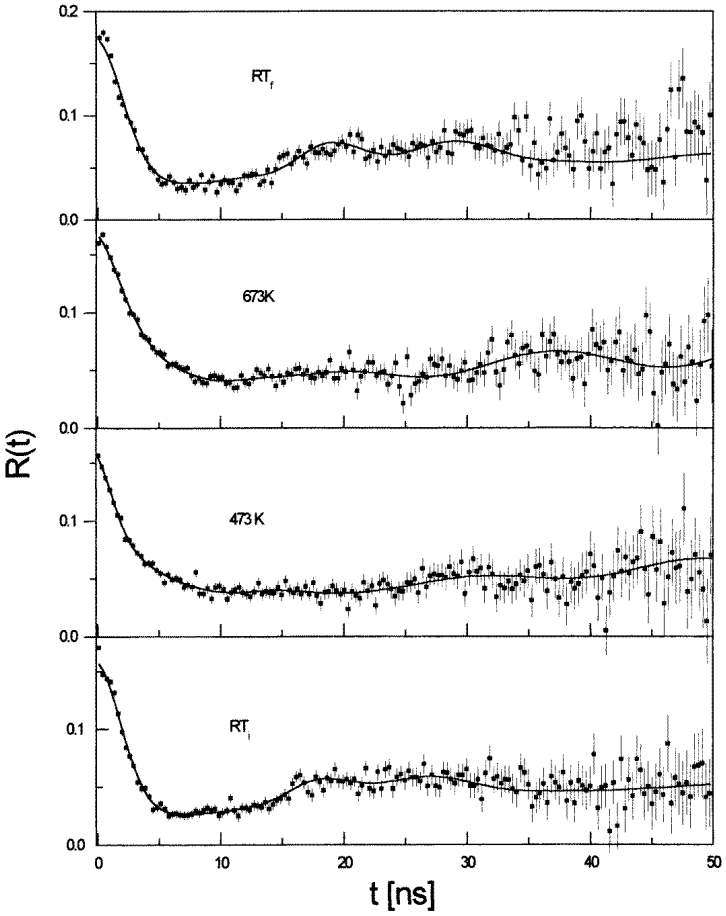

Figure 3. Spin-precession curves for PZT 9010 measured at different temperatures, corresponding to every phase. The RT_i spectrum is similar to the RT_f one, showing the phase reversibility.

3. PAC characterization

3.1. $PbZr_{0.9}Ti_{0.1}O_3$

In figure 3 we show some spin-precession curves obtained for a powder sample of $PbZr_{0.9}Ti_{0.1}O_3$ below and above the Curie temperature ($T_c \approx 528$ K), from RT to 873 K. These measurements were made while increasing the temperature up to the maximum value (873 K) and then decreasing it to some intermediate values and then down to RT. The function given by equation (2) was fitted to every spin-rotation curve. The best fits were obtained when the probes were allowed to occupy two sites over the whole temperature range. Attempts to adjust the data using a unique static quadrupole interaction were not satisfactory. Each site is characterized with a set of hyperfine parameters f, ω_q, η and δ. In figure 4 the fitted hyperfine parameters for sites 1 and 2 are plotted as functions of temperature. The regions established in the phase diagram shown in figure 1 are also included.

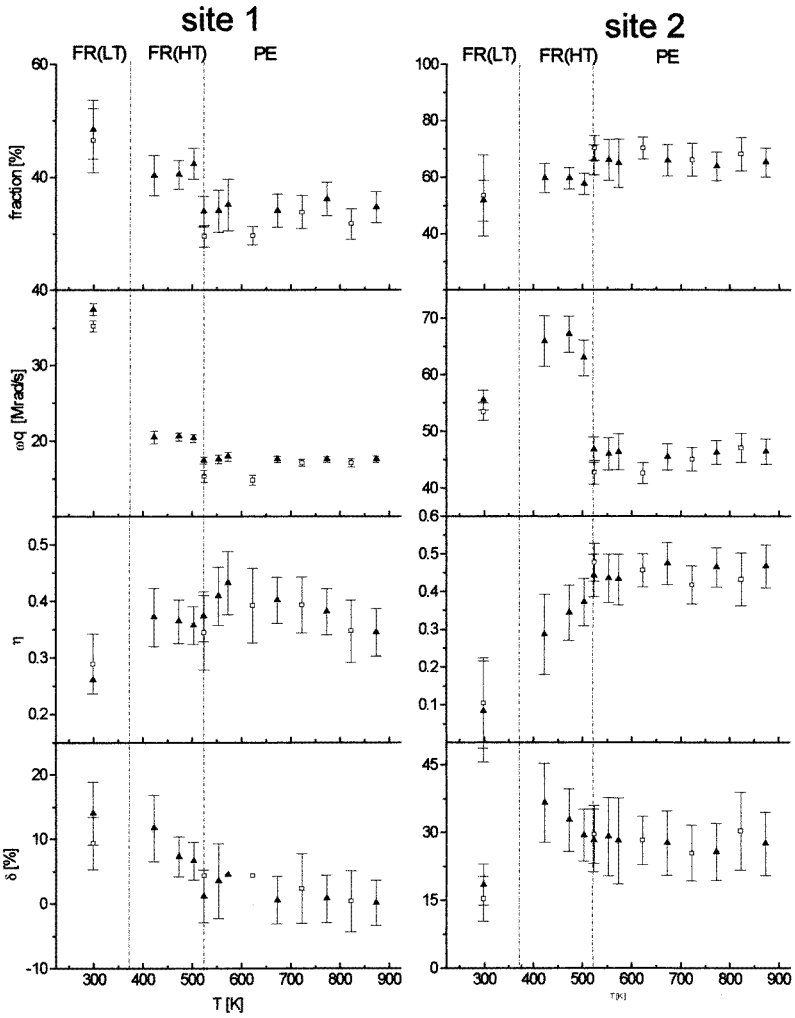

Figure 4. Fitted hyperfine parameters obtained as functions of temperature for PZT 9010. Triangles correspond to measurements made while increasing the temperature, while squares correspond to measurements made while decreasing the temperature. The dashed lines indicate the three different phases.

The populations of the two sites are nearly temperature independent, except for a step in the ferroelectric-to-paraelectric phase transition temperature (T_c), with average values of $f_1 \simeq 48\%$ and $f_2 \simeq 52\%$ in the FE phase and $f_1 \simeq 30\%$ and $f_2 \simeq 70\%$ in the PE phase.

Site 1 which we will also refer to as the low-frequency (LF) site is characterized at RT in the FR(LT) phase by $\omega_q = 37.4_7$ Mrad s^{-1}, $\eta = 0.26_3$ and $\delta = 0.14_1$. The temperature dependence of ω_q shows three regions corresponding to each phase. The value indicated above falls to 21 Mrad s^{-1} at temperatures from 423 to 503 K which corresponds to the FR(HT) phase. In the cubic phase, at 523 K and above, the frequency for this site decreases to nearly 17 Mrad s^{-1}. In the last two phases ω_q seems to be almost constant. The asymmetry parameter increases with temperature from $\eta \simeq 0.3$ at RT to $\eta \simeq 0.4$ in the cubic phase. The distribution parameter continuously decreases with temperature and is

nearly zero in the cubic phase, showing that this site is ordered.

For the high-frequency (HF) site, the hyperfine parameters at RT are $\omega_q = 55_1$ Mrad s^{-1}, $\eta = 0.08_2$ and $\delta = 0.18_4$. In the FR(HT) phase the quadrupolar frequency jumps to values close to 65 Mrad s^{-1}, and then falls to 45 Mrad s^{-1} for the cubic structure. In the ferroelectric phases the asymmetry parameter grows linearly with temperature, reaching the value of 0.37 just below the phase transition temperature. Above T_c it remains almost constant with an approximate value of $\eta = 0.43$. The distribution width parameter seems to be larger for the FR(HT) phase than for the FR(LT) phase. For the high-temperature cubic phase it is almost constant with a mean value of $\delta = 0.3$. This site is disordered at all temperatures.

Comparing the fitted parameters obtained for the initial and final RT measurements, it can be seen that the observed transitions are reversible.

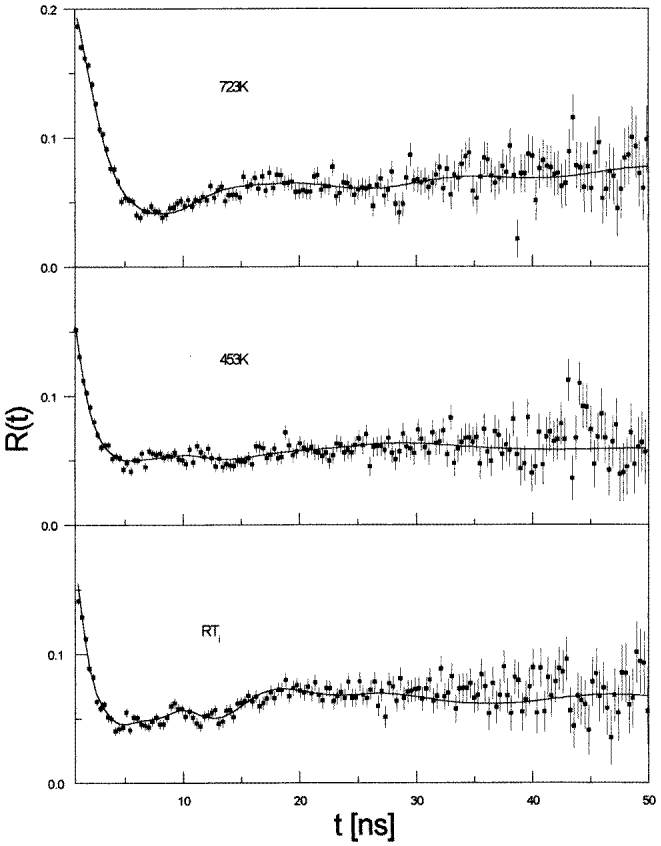

Figure 5. Spin-precession curves for PZT 8020 measured at different temperatures, corresponding to every phase.

3.2. $PbZr_{0.8}Ti_{0.2}O_3$

For this concentration the phase diagram (see figure 1) indicates that the Curie point T_c is close to 573 K, and that the transition from the FR(LT) phase to the FR(HT) phase occurs approximately at 413 K, i.e. both phase transition temperatures are higher than for

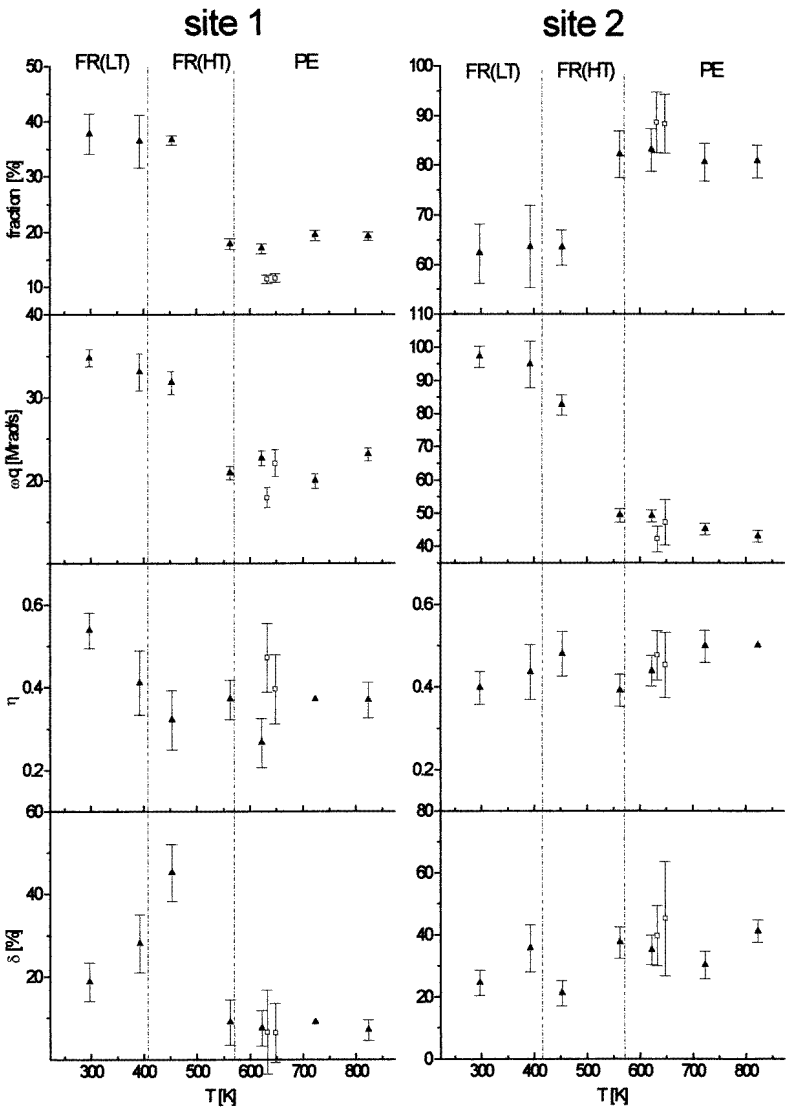

Figure 6. The fitted hyperfine parameters obtained as functions of temperature for PZT 8020. Triangles correspond to measurements made while increasing the temperature, while squares correspond to measurements made while decreasing the temperature. The dashed lines indicate the three different phases.

$PbZr_{0.9}Ti_{0.1}O_3$. In figure 5 several spin-rotation curves for this composition, corresponding to the three different phases, can be seen. For this compound, as for $PbZr_{0.9}Ti_{0.1}O_3$, the best fits are achieved if probes are supposed to occupy two sites. In figure 6, the fitted hyperfine parameters as functions of temperature are shown.

The temperature dependence of the f-values shows a clear step at T_c showing the same trend as was observed for $PbZr_{0.9}Ti_{0.1}O_3$. In the FR(LT) phase, site 1 is characterized by an almost constant frequency with $\omega_q \simeq 34$ Mrad s^{-1} which decreases to 18 Mrad s^{-1} for the FR(HT) phase. For both ferroelectric phases, while the temperature increases, the

asymmetry parameter decreases from about 0.53 to 0.4 and the distribution width parameter increases from ≈0.18 to 0.45.

In the cubic phase ($563 \leqslant T \leqslant 823$ K), the quadrupolar frequency and the asymmetry and distribution width parameters are constant with lower values than those measured for the FR phases. In particular, the fact that $\delta \approx 0$ indicates that this site is ordered.

For the second site, the values of the frequency ω_q for the ferroelectric phases are larger than those corresponding to $PbZr_{0.9}Ti_{0.1}O_3$. For the FR(LT) phase the value of ω_q is 97 Mrad s^{-1} and for the FR(HT) phase $\omega_q = 82$ Mrad s^{-1}. For this phase the asymmetry parameter is almost constant with a mean value of $\eta = 0.4$. As for $PbZr_{0.9}Ti_{0.1}O_3$, the distribution width parameter for site 2 is larger than that for site 1.

In the cubic phase the second site is characterized by almost temperature-independent hyperfine parameters with the mean values $\omega_q = 45$ Mrad s^{-1}, $\eta = 0.44$ and $\delta = 0.35$. Thus in the cubic phase, probes at this site detect an asymmetric and disordered EFG.

We observe from the determination of the hyperfine parameters a discrepancy in the temperature at which the phase transition from the rhombohedral to the cubic phase occurs with respect to the value given in reference [1]. As can be seen in figure 1, the Curie point for this concentration is nearly 573 K. However, in our experiment it is observed that the sample is in the cubic phase at least at 563 K. In our electronic set-up the stability as regards temperature is better than 1 K. The origin of this discrepancy is probably the different accumulation times in the two measurements. For TDPAC spectroscopy, the accumulation time is approximately one day, while dielectric and polarization measurements take only minutes.

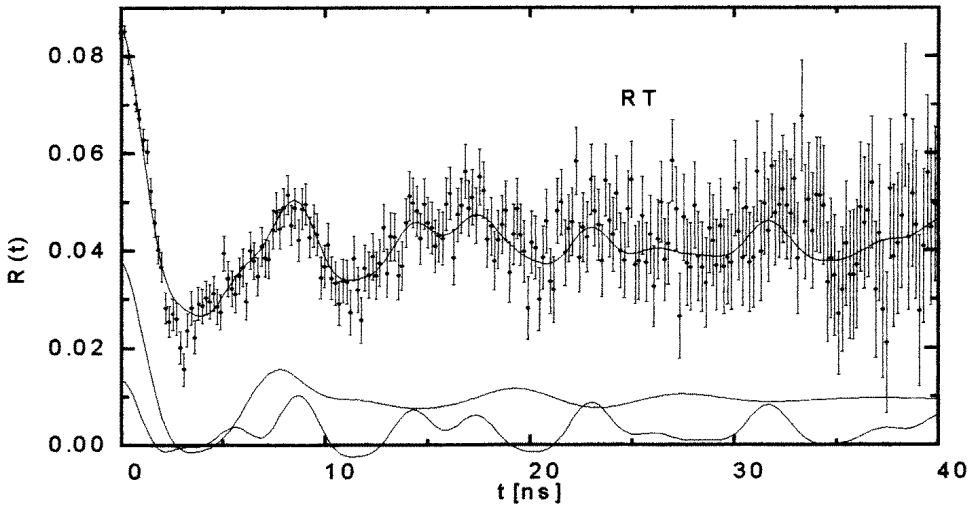

Figure 7. Spin-precession curves for PZT 6040 measured at RT. The lower curves show the fitted spin precessions corresponding to the two sites.

3.3. $PbZr_{0.6}Ti_{0.4}O_3$

The hyperfine parameters of this compound were determined at RT. In figure 7 the measured time spectrum is shown. For this concentration the phase transition from the FR(LT) phase to the FR(HT) phase is below RT, so this measurement at RT corresponds to the latter phase.

Again the best fit is obtained with probes at two sites with frequencies of 40_2 Mrad s^{-1} and 82_3 Mrad s^{-1}, respectively. The results are shown in table 1. The frequency of the first site is practically the same as the one corresponding to $PbZr_{0.8}Ti_{0.2}O_3$ at 453 K in its FR(HT) phase, while the frequency for the second site is larger. For the asymmetry parameters of the two sites, we note an increase in value with respect to those corresponding to the previously studied materials in the same phase. In the contrast, the disorder is slight.

Table 1. The hyperfine parameters for the different PZT compounds measured at RT.

Compound		Fraction (%)	ω_q (Mrad s^{-1})	η	δ (%)
$PbZr_{0.90}Ti_{0.10}O_3$	Site 1	48_5	37.4_7	0.26_3	14_4
	Site 2	52_7	55_1	0.08_2	18_4
$PbZr_{0.80}Ti_{0.20}O_3$	Site 1	37_3	34_1	0.53_4	18_4
	Site 2	62_6	97_3	0.39_3	24_4
$PbZr_{0.60}Ti_{0.40}O_3$	Site 1	35_3	40_2	0.68_7	3_1
	Site 2	65_{12}	82_3	0.63_6	14_5
$PbZr_{0.50}Ti_{0.50}O_3$*	Site 1	64_4	55_2	0	38_5
	Site 2	36_4	102_6	0	25_5

* Values obtained by Saxena *et al* [15].

3.4. $PbZrO_3$

The PZT family of compounds have two sharp changes in cell symmetries depending on Ti concentration. One of them is the morphotropic phase transition which is nearly temperature independent and occurs approximately when the percentage of Ti is 48%. At this concentration, the symmetry of the sample changes from rhombohedral to tetragonal. The other is at RT, when the Ti percentage is ≈6%. This transition is nearly temperature independent up to 473 K. For higher temperatures, the coexistence border tends towards smaller Ti concentration. In this case the line separates an antiferroelectric orthorhombic phase from a ferroelectric rhombohedral phase. The $PbZrO_3$ compound has already been studied by Forker and Hammesfahr using the PAC technique [13]. Their samples were prepared with already activated HfO_2 and measured by PAC spectroscopy below and above the transition temperature ($T_c = 503$ K).

Table 2. The hyperfine parameters measured for the FE phases $PbZrO_3$.

Temperature (ns^{-1})	Frequency (Mrad s^{-1})	Asymmetry	Distribution width	Relaxation
RT	49.2_8	0.85_4	0.06_2	—
523 K	—	—	—	0.044_7
RT*	54.96 ± 1.26	0.85 ± 0.02	0.08 ± 0.0073	—-
540 K	4.27 ± 0.27	—	—	—

* Values obtained by Forker and Hammesfahr [13].

We have also obtained PAC spectra of $PbZrO_3$ at the following temperatures: RT, 523 K and back at RT. The fitted hyperfine parameters obtained by us and those of Forker and Hammesfahr [13] are displayed in table 2. For the antiferroelectric phase the results of the two sets of measurements agree.

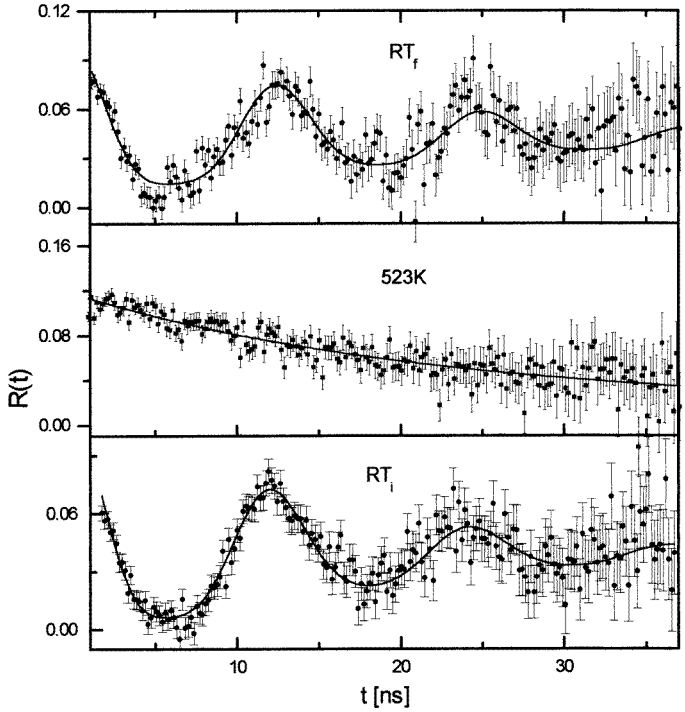

Figure 8. Spin-precession curves for $PbZrO_3$ measured for the antiferroelectric and PE phases.

When the transition to the cubic phase occurs, a big change in the correlation function is observed. In figure 8 the spin-precession data points and the fitted functions can be seen. Forker and Hammesfahr [13] adjusted their data for the cubic phase using a low and static EFG, obtaining a quadrupole frequency $\omega_q = 4.27_{27}$ Mrad s^{-1}. The fit of our time spectrum performed on the basis of the same model gave the following values: $\omega_q = 5.17_{1.33}$ Mrad s^{-1} and $\delta = 0.62_{26}$ if η is fixed at 1. For $\eta = 0$, $\omega_q = 6.12_{1.37}$ Mrad s^{-1} and $\delta = 0.59_{24}$. If the asymmetry parameter is not fixed at a value, the relative errors of the ω_q-, η- and δ-parameters are larger than 100%. Instead, in our case, the best fit is obtained with a relaxation process for this phase with $\lambda = 0.044_7$ ns^{-1}. Thus from these results, it can be seen that a unique fit is obtained with a relaxation model, and with only one free parameter. However, for a static process, different sets of parameters with large relative errors are possible.

4. Discussion

The crystalline structure of PZT 9010 has been studied by x-ray and neutron diffraction techniques at RT. These analyses show a superstructure characterized by oxygen octahedra rotations, alternately clockwise and anticlockwise, by 5.7° degrees along the polar axis. Each cell contains two formula units.

In a recent work based on TEM, dielectric spectroscopy, Sawyer–Tower polarization techniques and dilatometric measurements, Dai *et al* [14] proposed a modification in the Zr-rich zone of the existing PZT phase diagram. Based on the previous phase diagram, as shown in figure 1, the new one is subdivided into regions where different combinations of ordered

and disordered oxygen octahedral tilts of two distinct types would exist. For the FE(LT) phase an R-type oxygen octahedral rotational system associated with the condensation of a Γ_{25} optical phonon mode is proposed. Another type of oxygen octahedral rotation called M is associated with an instability of the M_3 optical phonon and determines the FE(HT) phase. Dai *et al* also proposed the existence of ordered and disordered M-type tilts.

In an independent work, Saxena *et al* [15] also observed two sites in $PbZr_{0.5}Ti_{0.5}O_3$ at RT in the tetragonal phase, using PAC spectroscopy and ^{181}Ta as probes. The hyperfine parameters (see table 1) obtained from the fit are $f_1 = 0.64_4$, $\omega_{q1} = 55_2$ Mrad s^{-1} and $\delta_1 = 38_5$% for the first site and $f_2 = 0.36_4$, $\omega_{q2} = 102_6$ Mrad s^{-1} and $\delta_2 = 25_5$% for the second site. For both sites the asymmetry parameter was fixed to zero, because a tetragonal symmetry was assumed for the lattice.

In the present work we also observe by PAC spectroscopy the presence of two distinct coexisting structures or sites for every PZT sample for which measurements were made. In the $PbZr_{0.9}Ti_{0.1}O_3$ compound, the three phases are observed through the variation with temperature of the quadrupole frequency, asymmetry, fraction and distribution width parameters. At RT the two sites are almost equally populated. With increasing temperature the population of the high-frequency site increases at the expense of the other. In the cubic phase, $f_1 \sim 35$% and $f_2 \sim 65$%. A final measurement, again at RT, yielded $f_1 \sim f_2 \sim 50$%.

The thermal behaviour of the hyperfine parameters at each site shows differences; while ω_{q1} for the FE(LT) phase is twice the value for the FR(HT) phase, ω_{q2} shows a 20% increase with respect to the RT value. The η-parameter shows almost the same thermal behaviour at both sites, but the distortion is larger for site 2. The distribution width parameter shows almost the same temperature dependence for the two sites, except that in the cubic phase, site 1 is ordered while site 2 is disordered.

For the $PbZr_{0.8}Ti_{0.2}O_3$ compound at RT, the fraction of site 2 is slightly larger than ~60%, and becomes ~85% for the cubic phase. At both sites the quadrupole frequency decreases with temperature. The asymmetry η is high at both sites and shows little temperature dependence. The distribution width parameters for the two sites display different behaviours with temperature. At RT they are practically equal ($\delta_1 \sim \delta_2 \sim 20$%), while for the PE phase the low-frequency site is nearly ordered and the high-frequency site is disordered.

The existence of EFGs in the cubic phases of both compounds must be discussed because it must be zero. We will consider this point below. Finally, the single measurement for the FR(HT) phase of $PbZr_{0.6}Ti_{0.4}O_3$ also shows two sites at RT. The populations and EFG parameters of the two sites appear to be in correspondence with those of PZT 9010 and 8020 for the same phase.

In the extreme cases of Ti substitution, $x = 1$ (Forker and Hammesfahr [13] and this work) and $x = 0$ (Catchen *et al* [16]), only one site is observed. For $PbZrO_3$ (PZ) and $PbTiO_3$ (PT) the hyperfine parameters at RT are $\omega_q = 55.0_1$ Mrad s^{-1}, $\eta = 0.85_2$, $\delta = 0.08_7$ and $\omega_q = 133_1$ Mrad s^{-1}, $\eta = 0.11_2$, $\delta = 0.09_2$ respectively. The quadrupole frequency for both compounds goes towards zero with temperature below the Curie point. This behaviour of the quadrupole frequency can be ascribed to the displacive distortion of the soft phonon. In the Zr-rich PZT solid solution compounds, two sites occupied by probes appear over the whole temperature range for which measurements were made. They are different from those indicated by the measurements for the pure PZ and PT compounds. This result eliminates the possibility of the existence of PZ-like and PT-like environments.

At RT, x-ray and neutron diffraction studies show superstructures that have double the unit cell. In this double cell, the two B sites have identical oxygen octahedra but, as mentioned before, with different signs of the rotation angle. Accordingly, for the TDPAC

technique these two sites should be equivalent, i.e. only one EFG should be observed. The detection by PAC spectroscopy of two sites with very different EFGs does not correspond to that description. Moreover, the detection of EFGs $\neq 0$ for the cubic phase with values lower than those for the FE phases would indicate that part of the EFGs observed for the FE phases do not only arise from the oxygen octahedral tilts, because those tilts disappear in the PE phase. Tentatively we can propose that the different sites observed originate from the presence of defects in the neighbourhood of probes. Oxygen vacancies have been observed to be produced during the heating of the ABO_3 compounds at high temperatures. Even though care has been taken during the preparation of PZT samples in order to guarantee stoichiometry, we cannot discard the possibility that there are lead vacancies. Thus oxygen and lead vacancies are the most probable defects expected. In the FE phases the oxygen tilts and the defects contribute to the EFGs. In the PE phases only defects produce EFGs.

In the work of Dai *et al* [14], in spite of the complexity of the problem of finding the most stable structures for PZT compounds, a modified phase diagram is proposed. This new diagram suggests that different structures (ordered or disordered R and M oxygen configurations) are possible which are energetically almost identical. Small changes in Ti concentration or temperature can induce the transformation from one configuration to another. This high sensitivity could of course depend on the sample preparation—especially that of the polarization-constricted state if oxygen vacancies are present and generated at this stage. The results shown in the work of Dai *et al*, which were obtained using macroscopic techniques, cannot be easily quantified and compared with the hyperfine parameters obtained by the microscopic PAC technique, especially if vacancies are taken into account. In spite of some discrepancies, due to the sensitivity of hyperfine interactions to defects close to probes, this PAC study complements those previous studies.

The EFG measured in the cubic high-temperature structure must be zero. Thus, the values measured at the two sites in both compounds would indicate the presence of defects close to probes. As we stated before, the most common defects in these materials are oxygen (v_O) and lead (v_{Pb}) vacancies, at sites $(\frac{1}{2}, \frac{1}{2}, 0)$ and $(1, 0, 0)$, respectively. In order to estimate the EFGs at the B sites produced by these defects we will use the point charge model (PCM) [17]. This model gives a reasonable approximation for η but not for V_{zz}. A simple or double vacancy in the oxygen or lead sublattices creates an axially symmetric EFG, i.e. $\eta = 0$. Thus $\eta \neq 0$ would indicate a more complex structure of defects. We will assume a defect composed of one v_O with one nearest-neighbour v_{Pb}. Configurations with higher numbers of vacancies are discarded. Because in these materials the charge of the A cations is 2, we take the same value for v_{Pb}. On the other hand, for v_O the covalence of the O–B bonds will be represented by a charge varying from 0 to 2. For this charge range the calculation gives $\eta \approx 0.40$ for v_O^1 and $v_O^{1.8}$ respectively. Even though the calculated V_{zz}s are not comparable to the experimental values, the ratio of the calculated V_{zz}-values for these charge configurations is $\sim$2.64, a value close to the ratio of the quadrupole frequencies. Thus, site 1 would correspond to a unique Ta–v_O^{1+}–v_{Pb}^{2-} configuration due to δ being approximately zero. The other site with the high V_{zz} and $\delta \approx 0.30$–0.40 would correspond to disordered Ta–$v_O^{1.8+}$–v_{Pb}^{2-} configurations.

If we assume randomly distributed vacancies there should exist some fraction of zero-frequency sites in the cubic phase. As this site is not detected, vacancies would be either close to Hf or migrate and become attracted by Ta. Since the Ta concentration is at the ppm level and the hyperfine parameters for every phase are constant as temperature varies, the second scenario seems improbable, unless the oxygen mobility at room temperature is high enough to enable the saturation of vacancy trapping to occur during the 17.8 microseconds of the Ta half-life.

In contrast, the first scheme, i.e. vacancies 'bound' to Hf, is probably more realistic and results from the lattice dynamics produced by O(2p) coupling to a mixture of [Zr(4d)–Hf(5d)]$_x$–[Ti(3d)]$_{1-x}$ orbitals. When the FE–PE phase transition occurs, the occupation of site 1 decreases by about 40% for $PbZr_{0.9}Ti_{0.1}O_3$ and $PbZr_{0.8}Ti_{0.2}O_3$. This transformation from one site to the other could take place if a charge transfer occurs during the phase transition. In this case the charges of oxygen vacancies for the FE phase would be different to those for the cubic phase. A better description of the EFG and charge distributions can be obtained if, instead of using the PCM, calculations like those of references [18] and [19] were made.

The line broadening detected in PZT and ABO_3 compounds [20] is a curious result. In most compounds it is related to disorder, and, in contrast to what happens in perovskites, the effect is annealed at high temperatures. Thus even though it could be related to defects, its nature is still not understood.

For the cubic phase of pure ABO_3 compounds it has been observed by PAC spectroscopy that probes are perturbed by a dynamic EFG, while samples with the formula $AB_xB'_{(1-x)}O_3$ show a static EFG. For example, $BaTiO_3$ [9] and $BaHfO_3$ [21] each show a hyperfine relaxation process in their respective cubic phases. The same result has been obtained for $PbZrO_3$ by us and for $PbTiO_3$ [16]. For $BaTiO_3$, $PbZrO_3$ and $PbTiO_3$ an abrupt change in the angular correlation function was observed, which shows that probes are perturbed by a static EFG below the Curie point and by a dynamic EFG above it. $BaHfO_3$ is cubic over the whole temperature range and presents a dynamic interaction at every temperature measured. Although the nuclear spin-relaxation model fits the data points better, the origin of such a process is still unknown. On the other hand, for the cubic phases of $BaTi_xHf_{(1-x)}O_3$ [21] and $PbZr_xTi_{(1-x)}O_3$ a static EFG was unambiguously observed.

In reference [13] and ultimately in reference [22], the time spectra measured above the Curie temperature were adjusted using a static and disordered EFG model. This topic is still under discussion because of the very large values for the distribution width parameter obtained (normally $\delta > 100\%$). It is hard to understand how the disorder in the atomic positions or composition could produce dispersion of the EFG values of a hundred per cent or even higher when for amorphous materials (completely disordered samples) it has been observed to be $\delta < 40\%$ [23].

In agreement with previous results obtained for other cubic ABO_3 samples, a nuclear spin-relaxation model is found to fit better the perturbation function obtained for the cubic structure of $PbZrO_3$. However, it is still difficult to imagine what physical process could be responsible for such a mechanism.

5. Conclusions

Powder samples of PZT for different Zr/Ti concentration ratios extending into the Zr-rich zone were analysed by XRD and PAC techniques. In the PZT samples two sites are occupied by probes from RT to 873 K. The detection of two sites in PZT and the characteristics of the static EFGs below T_c could presumably be explained in terms of different types of oxygen octahedron tilt and the presence of defects in the lattice, arising from the Zr–Ti ion substitution, and lead and oxygen vacancies. Above T_c the EFG would be produced by v_{Pb} and v_O with two different charge states. The origin of the residual interaction measured for cubic ABO_3 is still unknown and is probably related to defects. The nuclear spin-relaxation mechanism seems to be the most realistic process for describing that interaction.

Acknowledgments

This work was partially supported by Consejo Nacional de Investigaciones Científicas y Técnicas and Comisión de Investigaciones Científicas de la Provincia de Buenos Aires, Argentina.

References

[1] Shirane G, Suzuki K and Takeda A 1952 *J. Phys. Soc. Japan* **1** 12
[2] Shirane G and Takeda A 1952 *J. Phys. Soc. Japan* **1** 5
[3] Sawaguchi E 1953 *J. Phys. Soc. Japan* **8** 615
[4] Barnett H 1962 *J. Appl. Phys.* **33** 1606
[5] Michael C, Moreau J M, Achenbach G D, Gerson R and James W 1969 *Solid State Commun.* **7** 865
[6] Glazer A M and Mabud S A 1978 *Acta Crystallogr.* B **34** 1060
[7] Ito H, Shiozaki Y and Sawaguchi E 1982 *J. Phys. Soc. Japan* **52** 3913
[8] Comes R, Lambert M and Guinier A 1968 *Solid State Commun.* **9** 715
Comes R, Lambert M and Guinier A 1970 *Acta Crystallogr.* A **26** 244
[9] Catchen G L, Wukitch S J, Saylor E M, Huebner W and Blaszkiewicz M 1991 *Ferroelectrics* **117** 175
[10] Frauenfelder H and Steffen R M 1965 *Alpha-, Beta- and Gamma-Ray Spectroscopy* ed K Siegbahn (Amsterdam: North-Holland) p 997
[11] Butz T and Lerf A 1983 *Phys. Lett.* **97A** 217
[12] Abragam A and Pound R P 1953 *Phys. Rev.* **92** 953
[13] Forker M and Hammesfahr A 1972 *Z. Phys.* **255** 196
[14] Dai X, Xu Z and Viehland D 1995 *J. Am. Ceram. Soc.* **78** 2815
[15] Saxena R and Souza R 1996 private communication
[16] Catchen G L, Wukitch S J, Spaar D M and Blaszkiewicz M 1990 *Phys. Rev.* B **42** 1885
[17] López-García A 1990 *Magn. Reson. Rev.* **15** 119
[18] Singh D J 1994 *Ferroelectrics* **153** 186
[19] Fabricius G, Peltzer y Blanca E L, Rodríguez C O, Ayala A P, de la Presa P and López-García A 1997 *Phys. Rev.* B **55** 41
[20] Ayala A and López-García A 1996 *Ferroelectrics* **185** 1
Ayala A and López-García A 1996 *Hyperfine Interact.* C **1** 364
[21] López-García A, de la Presa P and Rodríguez A M 1991 *Phys. Rev.* B **44** 9708
Sebastian K C, Somayajulu D R S, Jaffrey S N A, Sharma S S and Varma J 1996 *Hyperfine Interact.* **99** 347
[22] Catchen G, Hollinger E and Rearick T 1996 *Z. Naturf.* a **51** 411
[23] Damonte L C, Mendoza Zeliz L A and López García A R 1992 *Phys. Rev.* B **46** 13 767